Hindawi Publishing Corporation
Mathematical Problems in Engineering
Volume 2013, Article ID 630798, 12 pages
http://dx.doi.org/10.1155/2013/630798

Research Article

Entropy Generation Analysis in a Variable Viscosity MHD Channel Flow with Permeable Walls and Convective Heating

A. S. Eegunjobi[1] and O. D. Makinde[2]

[1] *Department of Mathematics and Statistics, Polytechnic of Namibia, Namibia's University of Science and Technology, Private Bag 13388, 13 Storch Street, Windhoek, Namibia*
[2] *Institute for Advanced Research in Mathematical Modelling and Computation, Cape Peninsula University of Technology, P.O. Box 1906, Bellville 7535, South Africa*

Correspondence should be addressed to A. S. Eegunjobi; samdet1@yahoo.com

Received 18 February 2013; Revised 6 April 2013; Accepted 13 April 2013

Academic Editor: Tirivanhu Chinyoka

This paper examines the effects of the thermodynamic second law on steady flow of an incompressible variable viscosity electrically conducting fluid in a channel with permeable walls and convective surface boundary conditions. The nonlinear model governing equations are solved numerically using shooting quadrature. Numerical results of the velocity and temperature profiles are utilised to compute the entropy generation number and the Bejan number. The results revealed that entropy generation minimization can be achieved by appropriate combination of the regulated values of thermophysical parameters controlling the flow systems.

1. Introduction

Hydromagnetic channel flows have attracted the attention of many researchers due to their numerous engineering and industrial applications. Such flow can be found in magnetohydrodynamic (MHD) generator, geothermal reservoirs, cooling of nuclear reactors, petroleum reservoirs, accelerators, pumps, flow meter, astrophysics, metallurgy, crystal growth, magnetic filtration and separation, jet printers, and microfluidic devices [1]. Several researchers have discussed MHD fluid flow under various physical situations [2–4]. Lehnert [5] presented a theoretical investigation on the behavior of electrical conducting liquid under magnetic field. Makinde and Mhone [6] investigated the combined effect of transverse magnetic field and radiative heat transfer on unsteady flow of a conducting optically thin fluid through a channel filled with saturated porous medium and nonuniform wall temperature. Seth et al. [7] studied unsteady MHD Couette flow of a viscous incompressible electrically conducting fluid between two parallel porous plates in the presence of a transverse magnetic field. Agarwal [8] analyzed the effect of magnetic field on generalized Couette flow. The combined effects of variable viscosity and electrical conductivity on MHD generalized Couette flow and heat transfer were numerically investigated by Makinde and Onyejekwe [9].

Meanwhile, most industrial and engineering flow processes and thermal systems are unable to work at optimal level due to entropy production. Therefore, it is imperative to determine the factors that contributed to entropy generation in order to minimize their effects and maximize the flow system efficiency. The analysis of entropy generation minimization in a thermal system was pioneered by Bejan [10]. Thereafter, several researchers have theoretically studied entropy generation in thermal and flow systems under many physical situations [11–13]. Sahin and Ben-Mansour [14] reported a numerical solution of the entropy generation in a circular pipe. Hooman [15] studied the effects of different thermal boundary conditions on entropy generation in a microscale forced convection with velocity slip. The effect of Navier slip on entropy generation in a porous channel with suction/injection was investigated by Eegunjobi and

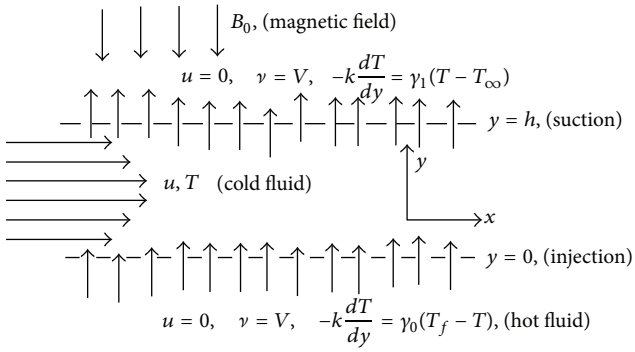

Figure 1: Schematic diagram of the problem.

Makinde [16]. Recently, Makinde and Eegunjobi [17] reported a numerical solution for the effects of convective heating on entropy production in a channel with permeable walls.

In this present study, the recent work of Makinde and Eegunjobi [17] is extended to include the combined effects of variable viscosity and asymmetric convective boundary conditions on the entropy generation rate in MHD porous channel flow. In the following sections, the model problem is formulated, analyzed, and numerically solved. Pertinent results are presented graphically and discussed quantitatively, with respect to various thermophysical parameters controlling the flow system.

2. Mathematical Model

We consider a steady, incompressible flow of an electrically conducting variable viscosity fluid between two fixed permeable parallel infinite plates of width h. The flow is fully developed and the edge effects are disregarded. A constant magnetic field of strength B_0 is imposed transversely in the y-direction. In addition, both the electric field and Hall effect are not present (see Seth et al. [7], Turkyilmazoglu [18]). The applied magnetic field is assumed to be strong enough so that the induced magnetic field due to the fluid motion is weak and can be neglected. It is assumed that the lower permeable plate, where fluid injection occurs, is convectively heated; while at the upper permeable plate both fluid suction and convective heat loss take place as shown in Figure 1.

Under these assumptions, the governing equations for the momentum and energy balance in one dimension can be written as follows [7–9, 16, 17]:

$$V\frac{du}{dy} = -\frac{1}{\rho}\frac{dP}{dx} + \frac{1}{\rho}\frac{d}{dy}\left(\overline{\mu}(T)\frac{du}{dy}\right) - \frac{\sigma B_0^2 u}{\rho}, \tag{1}$$

$$V\frac{dT}{dy} = \alpha\frac{d^2T}{dy^2} + \frac{\overline{\mu}(T)}{\rho c_P}\left(\frac{du}{dy}\right)^2 + \frac{\sigma B_0^2 u^2}{\rho c_p}. \tag{2}$$

The boundary conditions are

$$\begin{aligned} u(0) = 0, \quad -k\frac{dT}{dy}(0) &= \gamma_0\left(T_f - T(0)\right), \\ u(h) = 0, \quad -k\frac{dT}{dy}(h) &= \gamma_1\left(T(h) - T_\infty\right), \end{aligned} \tag{3}$$

where (x, y) is the axial and normal coordinates, u is the velocity of the fluid, P is the fluid pressure, V is the uniform suction/injection velocity at the channel walls, γ_0 is the heat transfer coefficient at the lower plate, γ_1 is the heat transfer coefficient at the upper plate, α is the thermal diffusivity, ρ is the fluid density, σ is the fluid electrical conductivity, k is the thermal conductivity coefficient, c_p is the specific heat at constant pressure, T_f is the temperature, of the hot fluid at the lower permeable plate, T is the channel fluid temperature, and T_∞ is the ambient temperature above the upper plate. The temperature dependent viscosity $\overline{\mu}$ can be expressed as [9]

$$\overline{\mu}(T) = \mu_0 e^{-m(T - T_\infty)}, \tag{4}$$

where m is a viscosity variation parameter and μ_0 is the fluid dynamic viscosity at the ambient temperature. We introduce the following nondimensional quantities:

$$\begin{aligned} &\eta = \frac{y}{h}, \qquad \alpha = \frac{k}{\rho c_p}, \qquad w = \frac{u}{V}, \\ &\theta = \frac{T - T_\infty}{T_f - T_\infty}, \qquad X = \frac{x}{h}, \qquad \overline{P} = \frac{ph}{\mu_0 V}, \\ &G = -\frac{\partial \overline{P}}{\partial X}, \qquad \mu = \frac{\overline{\mu}}{\mu_0}, \qquad \upsilon = \frac{\mu_0}{\rho}. \end{aligned} \tag{5}$$

Substituting (5) into (1)–(4), we obtain

$$\frac{d^2w}{d\eta^2} - \varepsilon\frac{d\theta}{d\eta}\frac{dw}{d\eta} - e^{\varepsilon\theta}\left(\mathrm{Re}\frac{dw}{d\eta} + \mathrm{Ha}\,w - G\right) = 0, \tag{6}$$

$$\frac{d^2\theta}{d\eta^2} - \mathrm{Re}\,\mathrm{Pr}\frac{d\theta}{d\eta} + \mathrm{Ec}\,\mathrm{Pr}\,e^{-\varepsilon\theta}\left(\frac{dw}{d\eta}\right)^2 + \mathrm{Ec}\,\mathrm{Pr}\,\mathrm{Ha}w^2 = 0, \tag{7}$$

with the boundary conditions

$$\begin{aligned} w(0) = 0, \quad \frac{d\theta}{d\eta}(0) &= \mathrm{Bi}_0\left(\theta(0) - 1\right), \\ w(1) = 0, \quad \frac{d\theta}{d\eta}(1) &= -\mathrm{Bi}_1\theta(1), \end{aligned} \tag{8}$$

where G is the pressure gradient parameter,

$\mathrm{Re} = Vh/\upsilon$ (Reynolds number),

$\mathrm{Pr} = \upsilon/\alpha$ (Prandtl number),

$\mathrm{Ec} = V^2/c_p\,(T_f - T_\infty)$ (Eckert number),

$\mathrm{Ha} = \sigma B_0^2\, h^2/\mu_0$ (magnetic field parameter or square of Hartmann number),

$\varepsilon = m(T_f - T_\infty)$ (variable viscosity parameter),
$\mathrm{Bi}_0 = \gamma_0 h/k$ (lower plate Biot number),
$\mathrm{Bi}_1 = \gamma_1 h/k$ (upper plate Biot number).

It is important to note that $\varepsilon = 0$ corresponds to the case of constant viscosity conducting fluid. The exact solution of (6) for the fluid velocity is possible under this constant viscosity scenario and we obtain

$$w(\eta) = \frac{G}{\mathrm{Ha}}\left[\frac{e^{\alpha\eta}\left(e^{\beta}-1\right) - e^{\beta\eta}\left(e^{\alpha}-1\right)}{e^{\alpha}-e^{\beta}} + 1\right], \quad (9)$$

where $\alpha = (\mathrm{Re} + \sqrt{\mathrm{Re}^2 + 4\mathrm{Ha}})/2$ and $\beta = (\mathrm{Re} - \sqrt{\mathrm{Re}^2 + 4\mathrm{Ha}})/2$. Moreover, the coupled nonlinear boundary value problem represented by (6)-(7) together with their boundary conditions in (8) has been solved numerically using an efficient fourth-order Runge–Kutta method along with a shooting technique [19].

3. Entropy Analysis

In many engineering and industrial processes, entropy production destroys the available energy in the system. It is therefore imperative to determine the rate of entropy generation in a system, in order to optimize energy in the system for efficient operation in the system. The convection process in a channel is inherently irreversible and this causes continuous entropy generation. Wood [11] gave the local volumetric rate of entropy generation for a viscous incompressible conducting fluid in the presence of magnetic field as follows:

$$E_G = \frac{k}{T_\infty^2}\left(\frac{dT}{dy}\right)^2 + \frac{\mu}{T_\infty}\left(\frac{du}{dy}\right)^2 + \frac{\sigma B_0^2}{T_\infty}u^2. \quad (10)$$

In (10), the first term represents irreversibility due to heat transfer; the second term is entropy generation due to viscous dissipation, while the third term is local entropy generation due to the effect of the magnetic field (Joule heating or Ohmic heating). Using (5), the dimensionless form of local entropy generation rate in (10) is given as follows:

$$\mathrm{Ns} = \frac{T_\infty^2 h^2 E_G}{k\left(T_f - T_\infty\right)^2} = \left(\frac{d\theta}{d\eta}\right)^2 + \frac{\mathrm{Br}}{\Omega}\left[e^{-\varepsilon\theta}\left(\frac{dw}{d\eta}\right)^2 + \mathrm{Ha}w^2\right], \quad (11)$$

where $\Omega = (T_f - T_\infty)/T_\infty$ is the temperature difference parameter and $\mathrm{Br} = \mathrm{Ec}\,\mathrm{Pr}$ is the Brinkmann number. The Bejan number (Be) is defined as

$$\mathrm{Be} = \frac{N_1}{N_s} = \frac{1}{1+\Phi}, \quad (12)$$

where $N_s = N_1 + N_2$, $N_1 = (d\theta/d\eta)^2$ (heat transfer irreversibility due to heat transfer), $N_2 = (\mathrm{Br}/\Omega)[e^{-\varepsilon\theta}(dw/d\eta)^2 + \mathrm{Ha}w^2]$ (fluid friction and magnetic field irreversibility), $\Phi = N_2/N_1$ (irreversibility ratio).

The Bejan number (Be) as shown in (12) has a range of $0 \le \mathrm{Be} \le 1$. If Be = 0, then the irreversibility is dominated by the combined effects of fluid friction and magnetic fields, but if Be = 1, then the irreversibility due to heat transfer dominates the flow system by the virtue of finite temperature differences.

Table 1: Comparison between the exact and numerical solution of velocity profile for $G = 1$, Re = 1, Ha = 1, and $\varepsilon = 0$.

η	Exact solution $w(\eta)$	Numerical solution $w(\eta)$
0	0	0
0.1	0.035822	0.035822
0.2	0.065264	0.065264
0.3	0.087963	0.087963
0.4	0.103449	0.103449
0.5	0.111127	0.111279
0.6	0.110257	0.110257
0.7	0.099930	0.099930
0.8	0.079042	0.079042
0.9	0.046264	0.046264
1.0	0	0

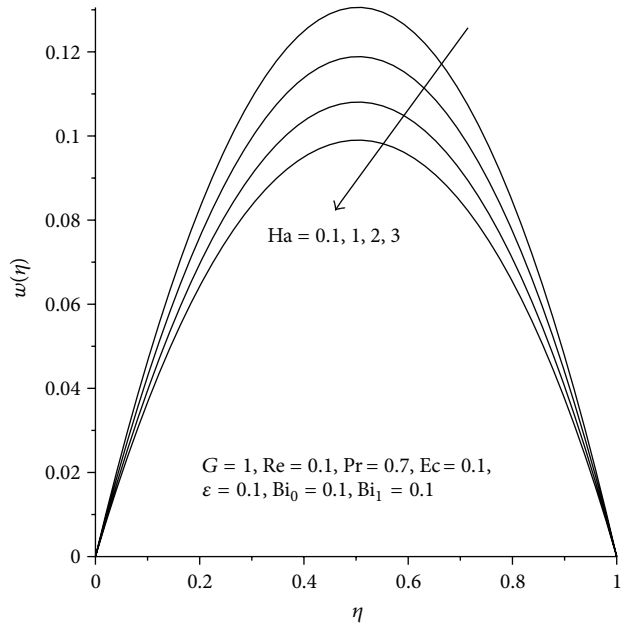

Figure 2: Velocity profiles increasing Ha.

4. Results and Discussion

The numerical results for the fluid velocity, temperature, entropy generation rate, and Bejan number distributions are reported in Table 1 and Figures 2–30. Representative values of various parameters are utilized and the Prandtl number Pr is assumed to range from 0.71 (Air) ≤ Pr ≤ 7.1 (water). In order to validate the accuracy of our numerical procedure, we compare a special case of our result ($\varepsilon = 0$) with the exact solution for the velocity profile in (9). The results displayed in Table 1 show perfect agreement and attest the correctness of our results.

4.1. Effects of Parameter Variations on Velocity Profiles. The effects of variation in key parameters on the velocity profiles are shown in Figures 2–8. Generally, the velocity profiles are parabolic in geometries with zero values at the channel

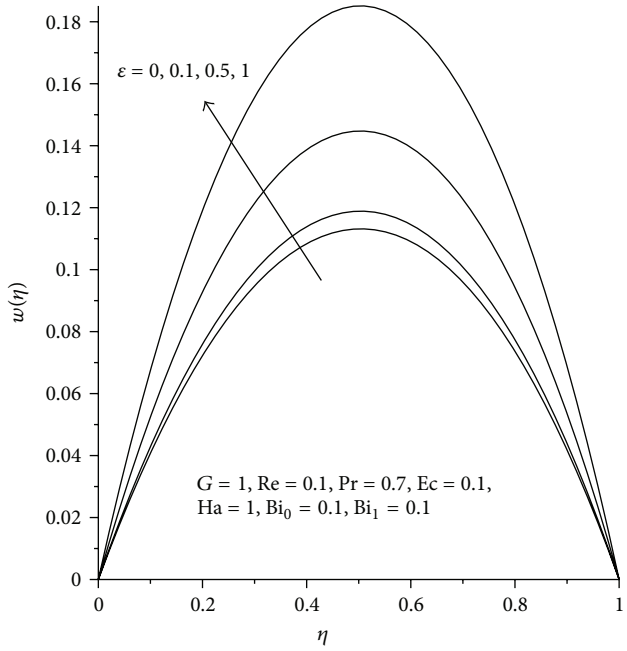

Figure 3: Velocity profiles increasing ε.

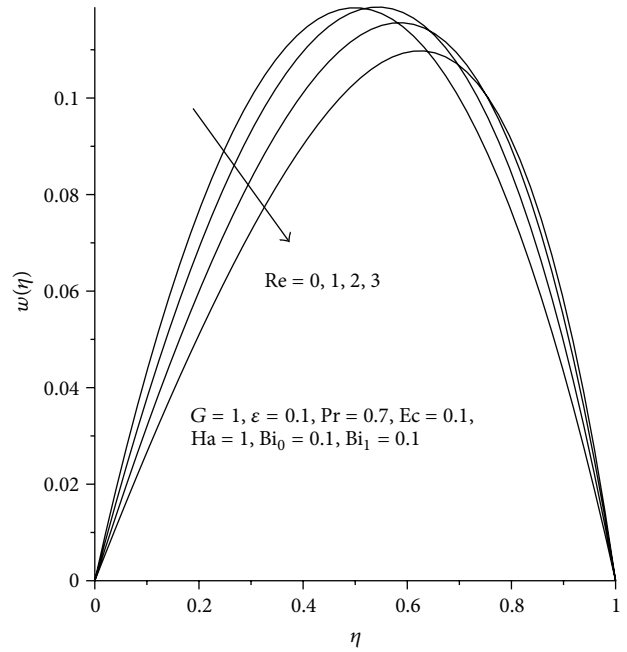

Figure 4: Velocity profiles with increasing Re.

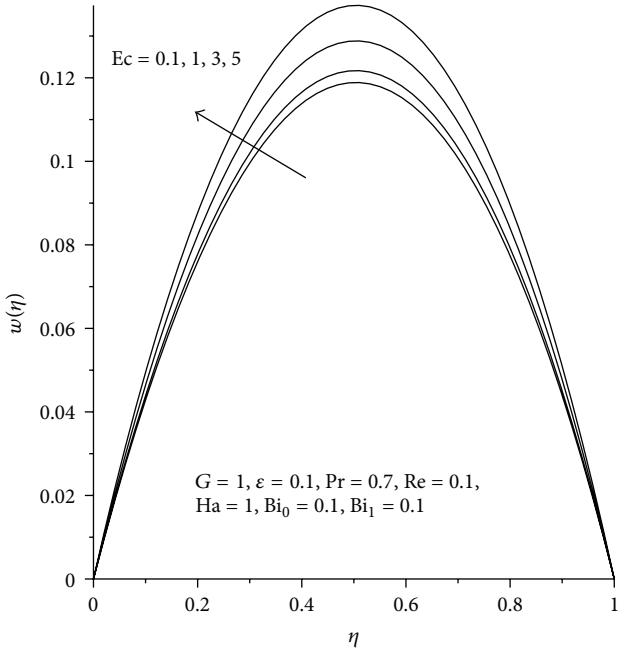

Figure 5: Velocity profiles with increasing Ec.

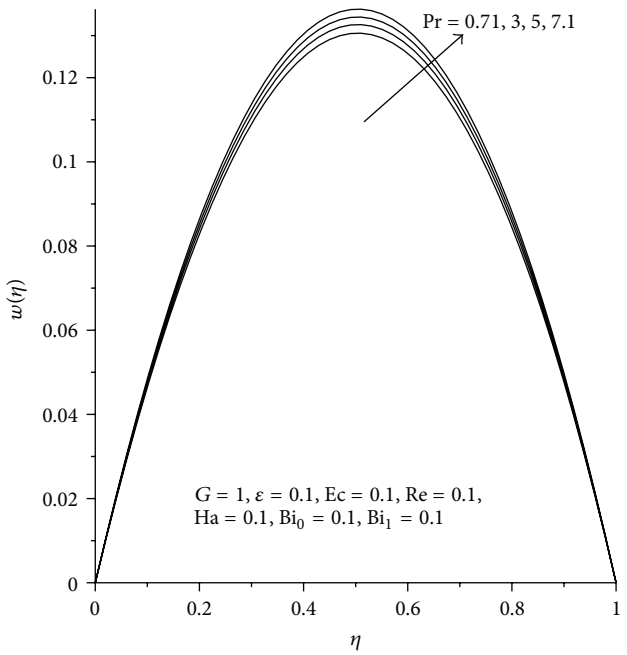

Figure 6: Velocity profiles increasing Pr.

walls due to no slip condition and attain their maximum value within channel. In Figure 2, it is observed that the fluid velocity decreases with increasing magnetic field intensity (Ha). This can be attributed to the presence of Lorentz force acting as a resistance to the flow as expected and is in perfect agreement with earlier results as reported in the literature [3–9]. As the fluid viscosity decreases as shown in Figure 3 with increasing values of ε, the velocity profiles increase. The fluid velocity decreases and skews towards the upper plate as Reynolds number (Re) increases due to increasing injection at the lower plate and increasing suction at the upper plate as shown in Figure 4. Figures 5 and 6 show that the fluid velocity increases with increase in the values of Eckert number (Ec) and Prandtl number (Pr). As Ec increases, the velocity gradient increases as a result of a decrease in the fluid viscosity, consequently, the fluid velocity increases. Figures 7 and 8 show that the fluid velocity increases with increasing convective heating (Bi_0) at the lower plate and decreases with

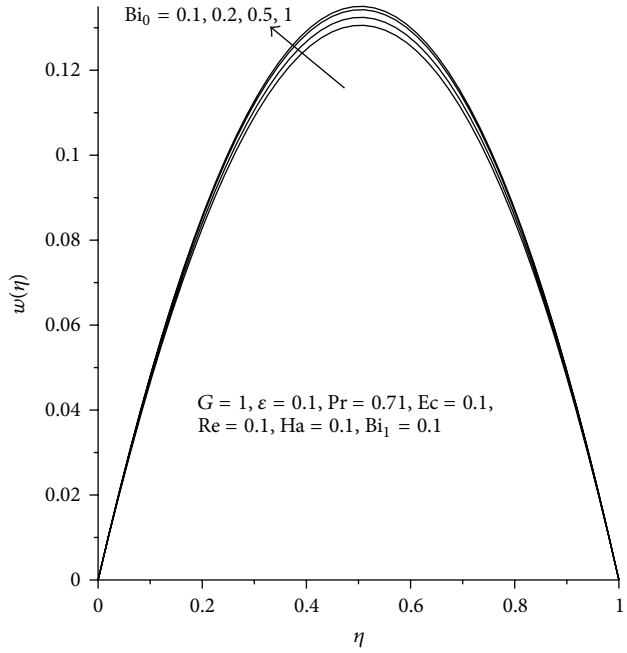

Figure 7: Velocity profiles with increasing Bi$_0$.

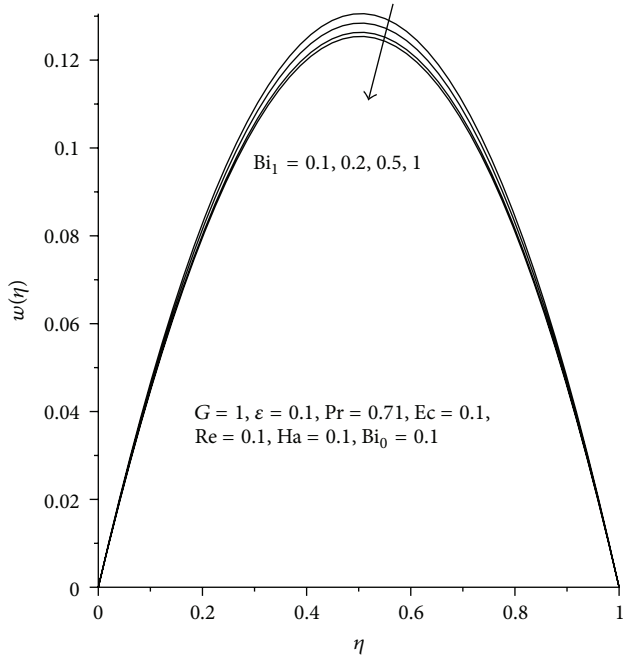

Figure 8: Velocity profiles with increasing Bi$_1$.

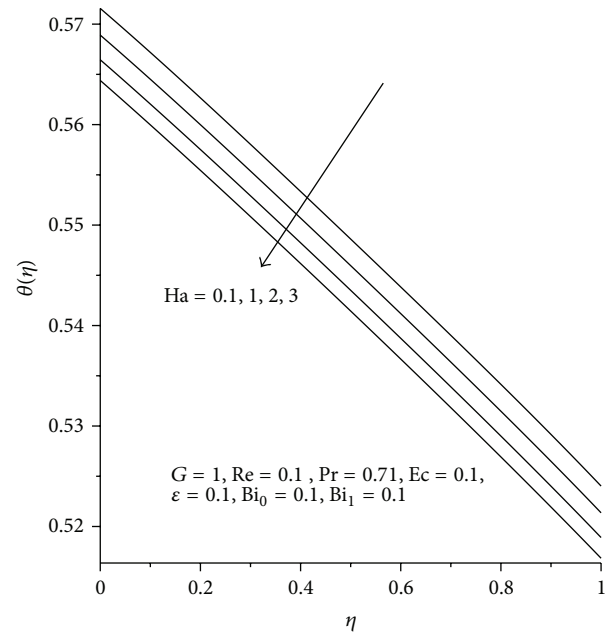

Figure 9: Temperature with increasing Ha.

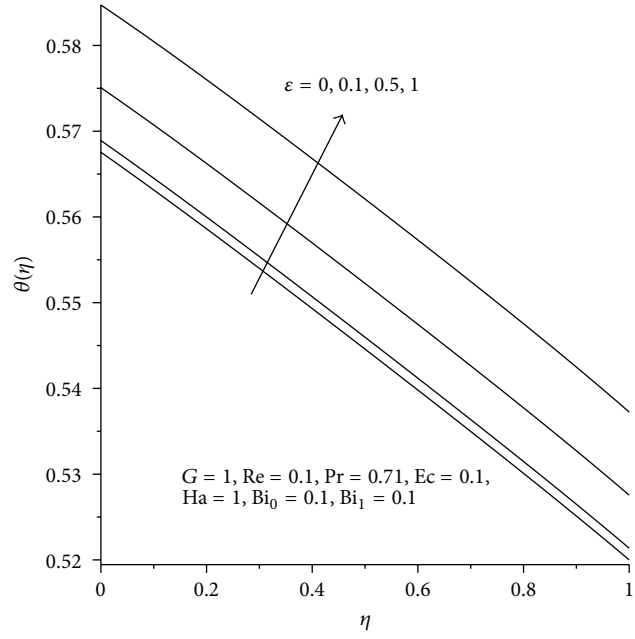

Figure 10: Temperature with increasing ε.

increasing convective cooling (Bi$_1$) at the upper plate. This is expected, since the fluid becomes lighter and flows faster with increasing temperature due to convective heating.

4.2. Effects of Parameter Variations on Temperature Profiles. Figures 9–15 demonstrate the effects of various parameters on the temperature profiles. The imposed thermal boundary conditions ensure that the fluid temperature at the lower plate is highest due to convective heating and decreases gradually to its lowest value at the upper plate due to convective heat loss to the ambient. Figure 9 shows the influence of magnetic field (Ha) on the flow field. As Ha increases due to increasing magnetic field intensity, the fluid temperature decreases within the channel. This decrease in the fluid temperature may be attributed to the combined effects of fluid suction and convective heat loss, despite the presence of Ohmic heating (or Lorentz heating) which serves as additional heat source to the flow system. The effects of increasing ε, Re,

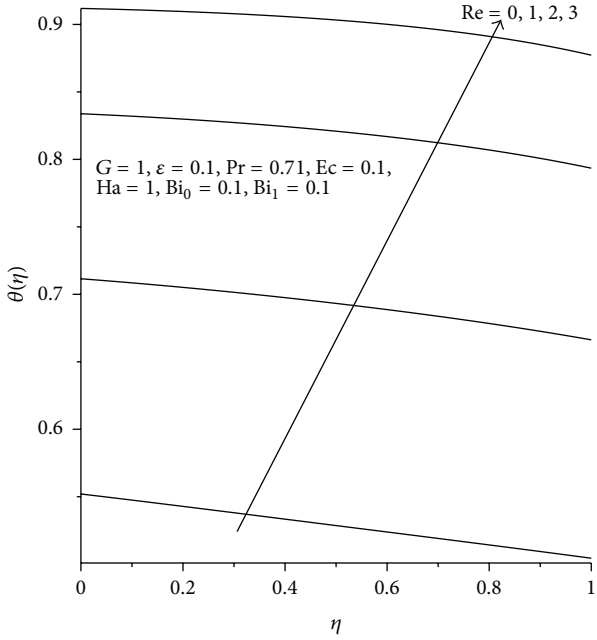

Figure 11: Temperature with increasing Re.

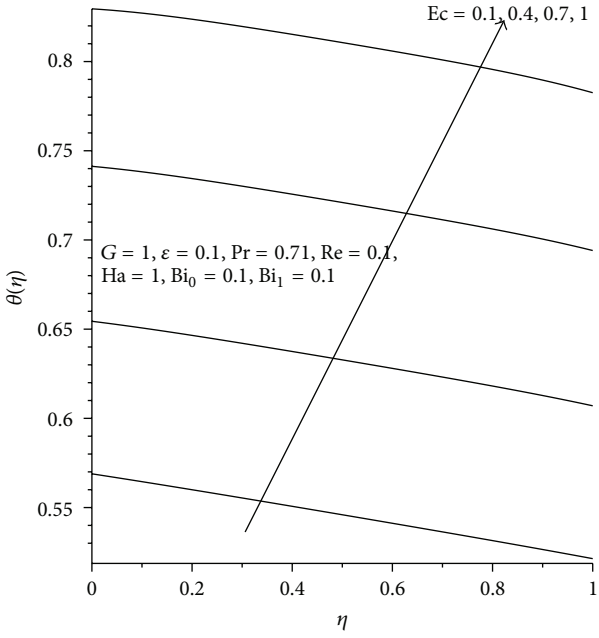

Figure 12: Temperature with increasing Ec.

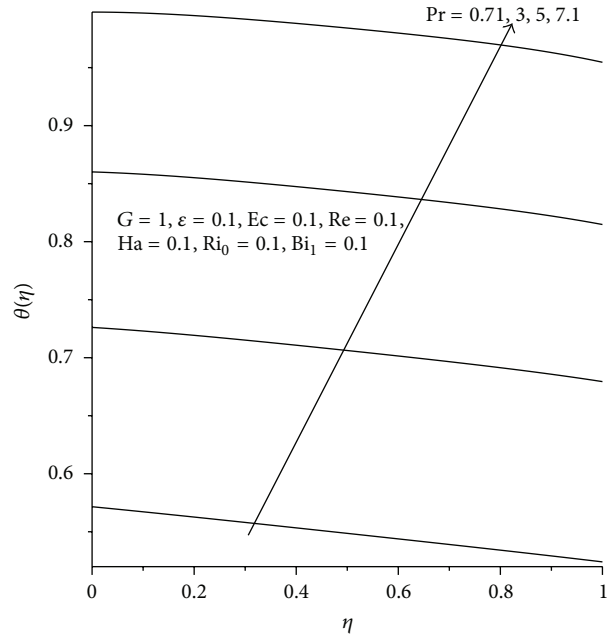

Figure 13: Temperature with increasing Pr.

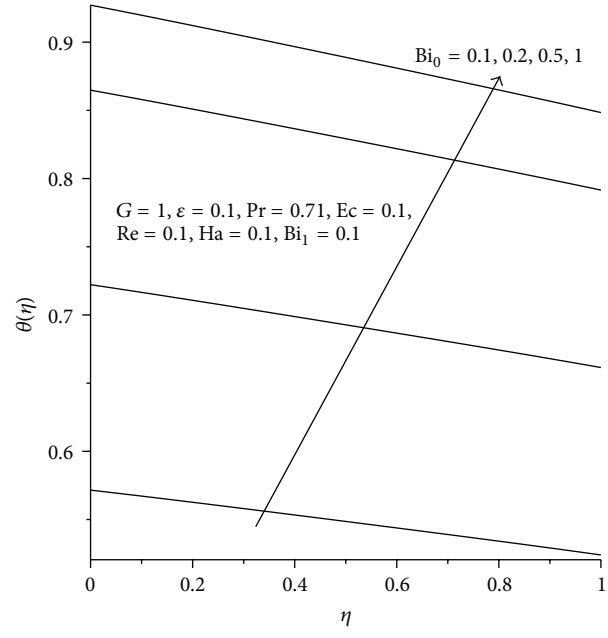

Figure 14: Temperature with increasing Bi_0.

and Ec are shown in the Figures 10, 11, and 12. The rise in the fluid temperature is observed with increasing values of these parameters. This may be attributed to the facts that as ε, Re, and Ec increase, the fluid viscosity becomes lighter and viscous heating increases due to increasing convective heating at the lower plate increases leading to a rise in the fluid temperature. As the Prandtl number increases from Pr = 0.71 (Air) to Pr = 7.1 (water) the fluid temperature decreases as illustrated in Figure 13. In Figure 14, a rise in the fluid temperature is observed with increasing convective heating at the lower plate as expected. Figure 15 shows the effect of increasing Bi_1 on the temperature. As expected, the fluid temperature decreases due to increasing convective heat loss at the upper plate.

4.3. Effects of Parameter Variations on Entropy Generation Rate. The effects of key parameters variation on entropy generation rate (Ns) are shown in Figures 16–22. Generally, the entropy production is more pronounced at the permeable channel walls and decreases towards the channel centerline

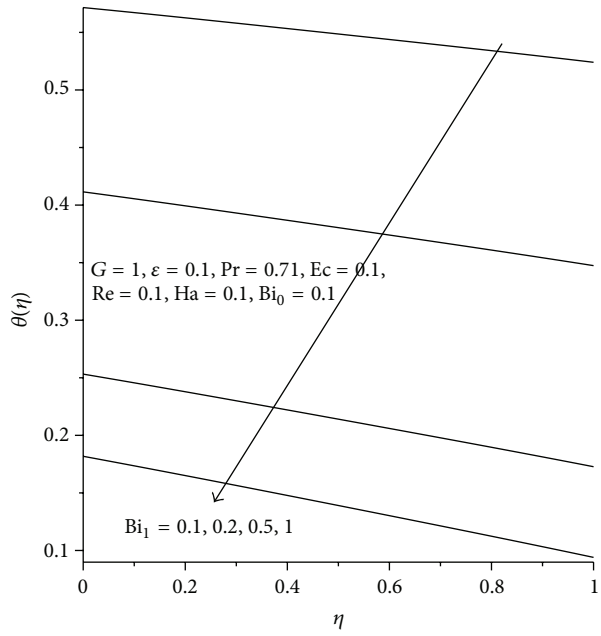

FIGURE 15: Temperature with increasing Bi_1.

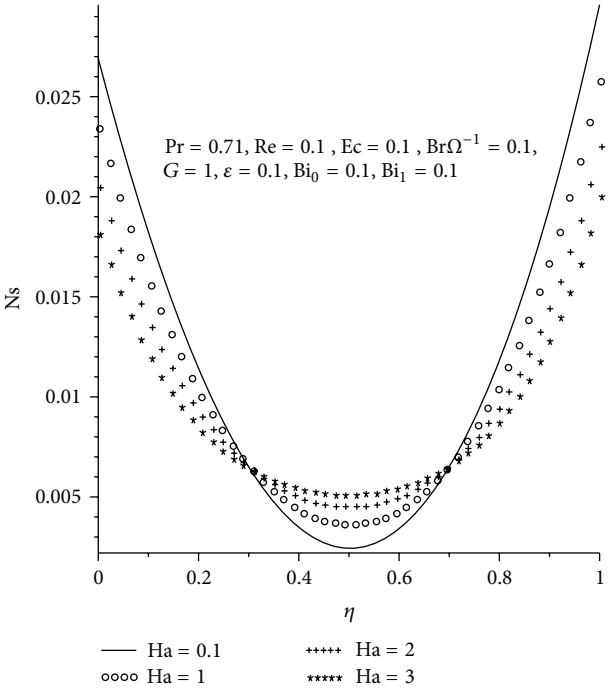

FIGURE 16: Ns with increasing Ha.

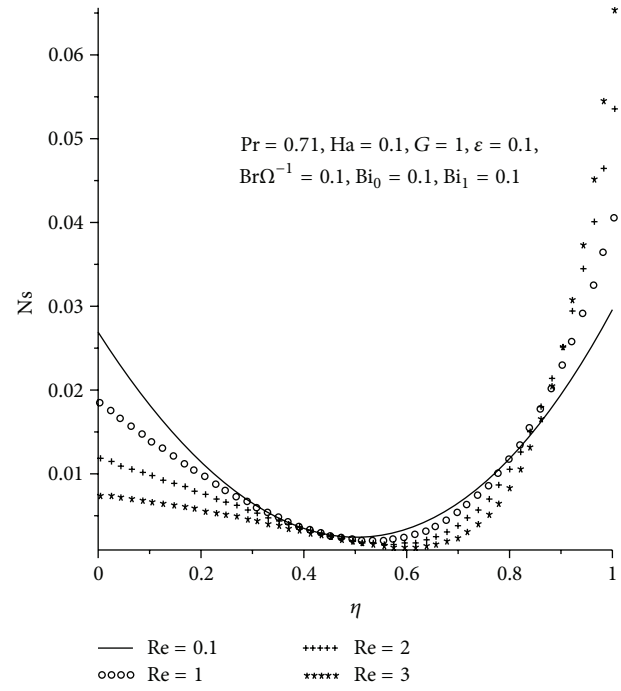

FIGURE 17: Ns with increasing Re.

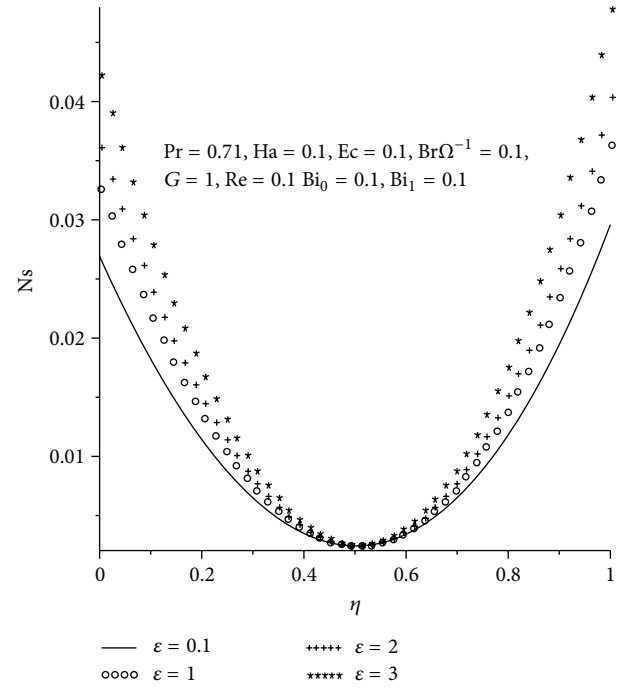

FIGURE 18: Ns with increasing ε.

region. Figure 16 reveals the effect of increasing magnetic field intensity (Ha) on entropy generation rate (Ns). As Ha increases, the entropy generation decreases at the walls and increases at the centerline region of the channel. Meanwhile, it is interesting to note that two points exist, that is, $\eta = 0.3$ and $\eta = 0.7$ within the flow field where the entropy production is not affected by increasing Ha. In Figure 17, it is observed that entropy production is enhanced with increasing suction (Re) at the upper wall region, while a decrease in the entropy generation occurs at the lower wall with increasing fluid injection. The effects of ε, $\mathrm{Br}\Omega^{-1}$ and G on the entropy generation rate are shown in Figures 18–20. As the fluid viscosity decreases with increasing values of ε,

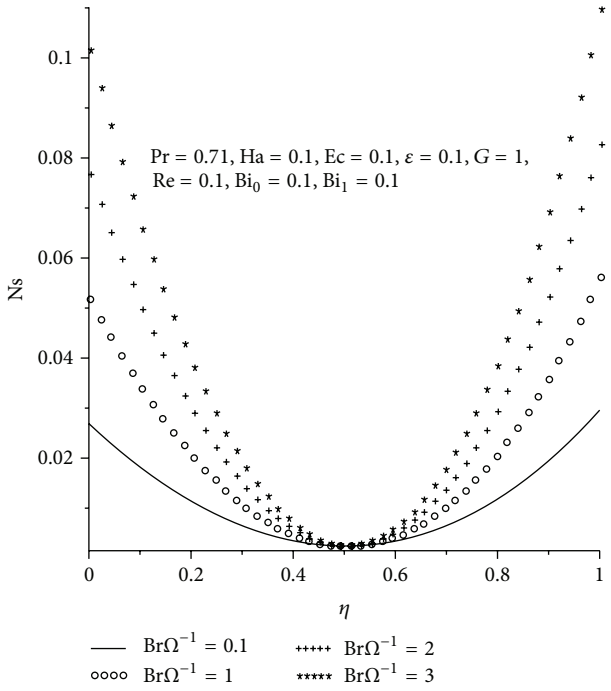

Figure 19: Ns with increasing $\mathrm{Br}\Omega^{-1}$.

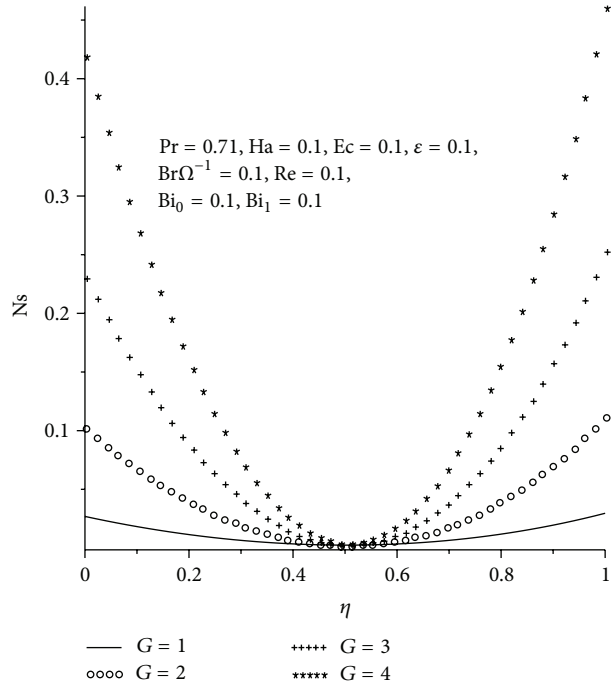

Figure 20: Ns with increasing G.

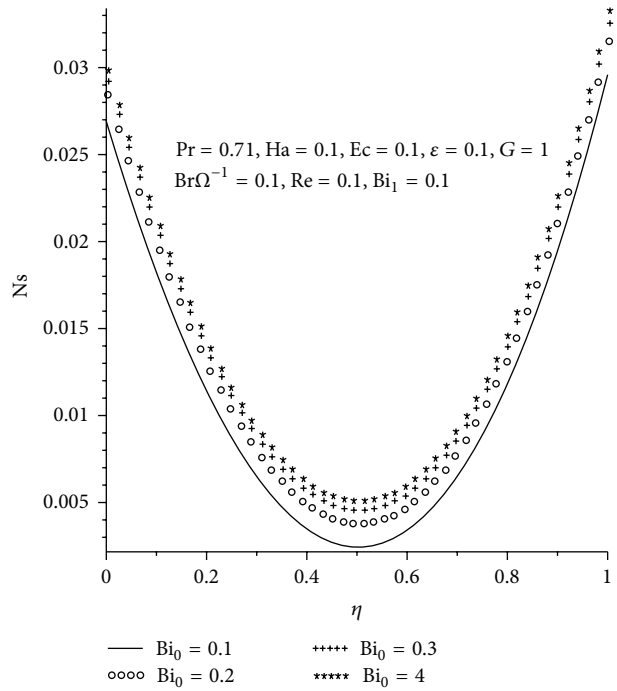

Figure 21: Ns with increasing Bi_0.

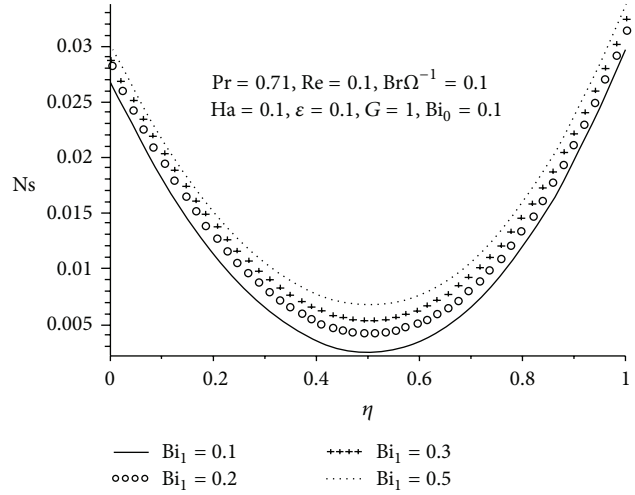

Figure 22: Ns with increasing Bi_1.

the entropy production increases at both walls and decreases towards the channel centerline as indicated in Figure 18. However, a point exists at $\eta = 0.5$, where entropy production is virtually zero. This may be attributed to the presence of zero velocity gradients at the region. A similar trend of entropy production is observed with increasing values of group parameter ($\mathrm{Br}\Omega^{-1}$) and constant pressure gradient (G) as demonstrated in Figures 19 and 20. Figures 21 and 22 show that the entropy generation rate increases with combined increase in convective heating at the lower wall and convective cooling at the upper wall that is, as Bi_0 and Bi_1 increase.

4.4. Effects of Parameter Variations on Bejan Number. Figures 23–30 illustrate the effects of different values of key parameters on Bejan number (Be). Generally, the Bejan number is highest along the channel centerline region with irreversibility due to heat transfer dominating the flow, while near the channel walls the fluid friction and magnetic field

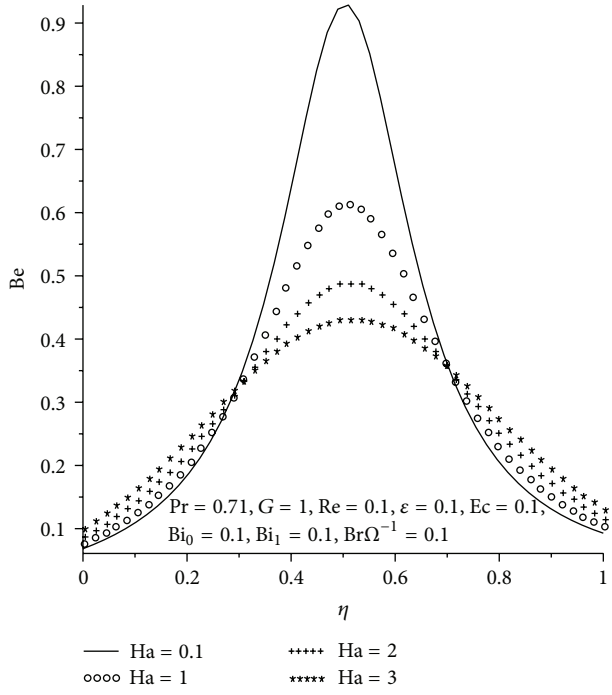

Figure 23: Bejan number with increasing Ha.

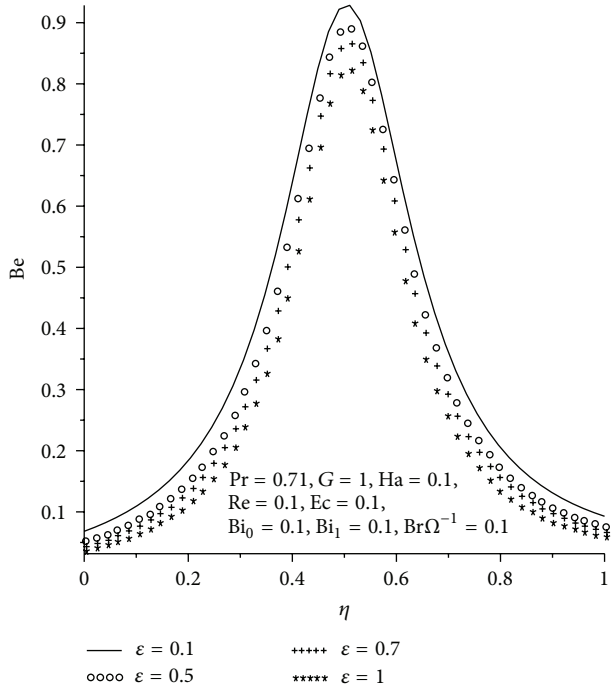

Figure 25: Bejan number with increasing ε.

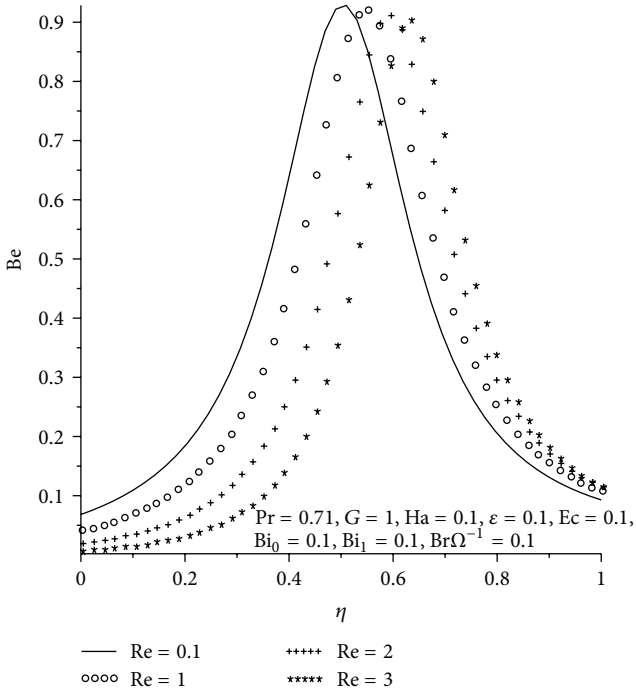

Figure 24: Bejan number with increasing Re.

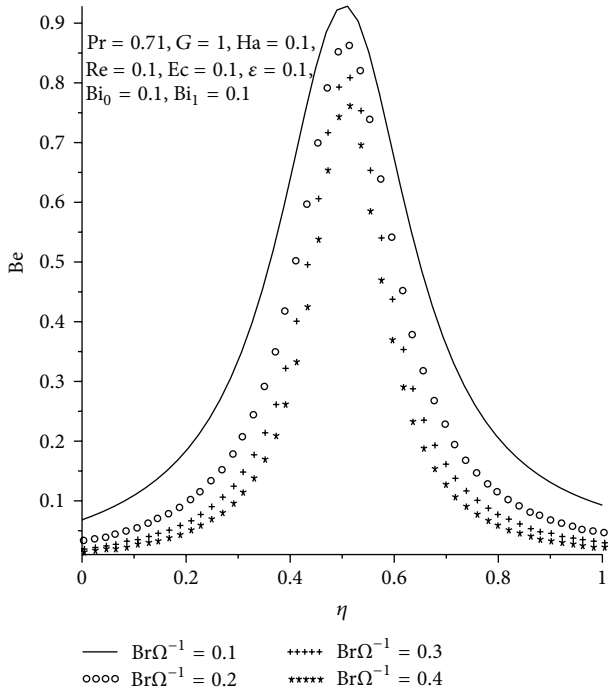

Figure 26: Bejan number with increasing $\mathrm{Br}\Omega^{-1}$.

irreversibility dominate. Moreover, it is evident in Figure 23 that an increase in Ha results in a decrease of Be along the channel centerline. As Re increases (see Figure 24), the Bejan number decreases near the lower wall due to injection and increases toward the upper wall due to suction. Figures 25 and 26 show a general decrease in Bejan number with increasing parameter values of ε and $\mathrm{Br}\Omega^{-1}$ due to a decrease in fluid viscosity and an increase in viscous dissipation irreversibility. In Figures 27 and 28, an increase in the dominant influence of heat transfer irreversibility is observed as the parameter values of Bi_0 and Bi_1 increase, consequently, the Bejan number increases. Hence, the convective thermal boundary

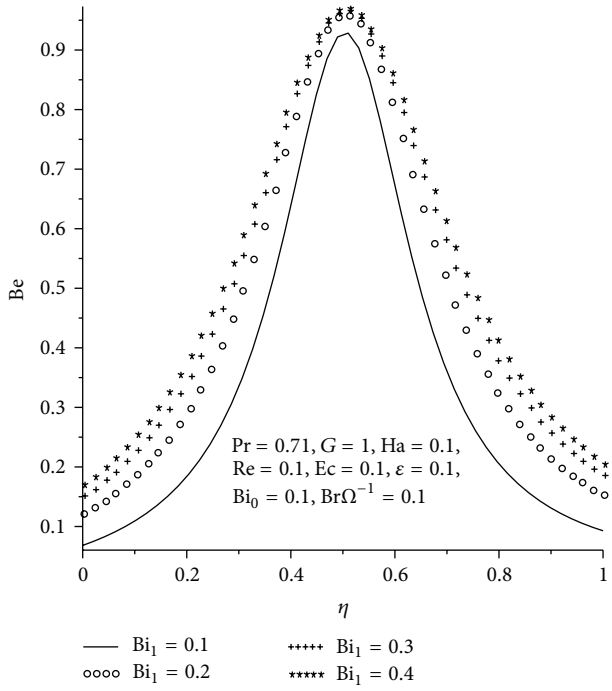

Figure 27: Bejan number with increasing Bi_1.

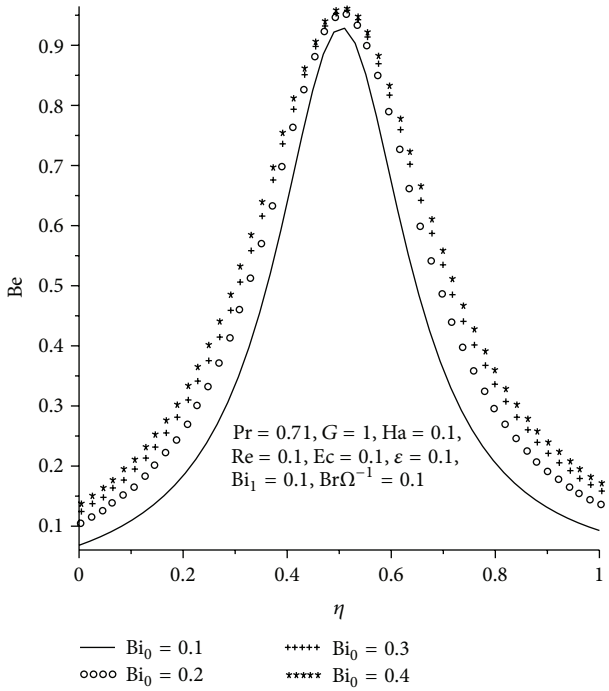

Figure 28: Bejan number with increasing Bi_0.

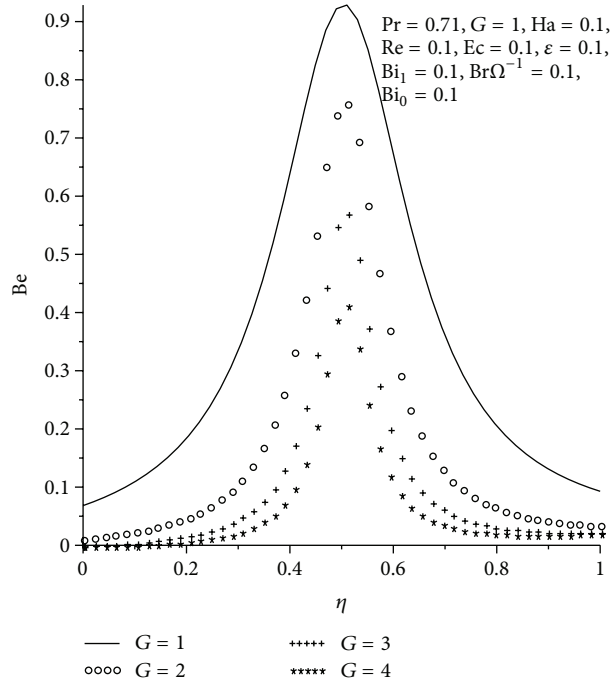

Figure 29: Bejan number with increasing G.

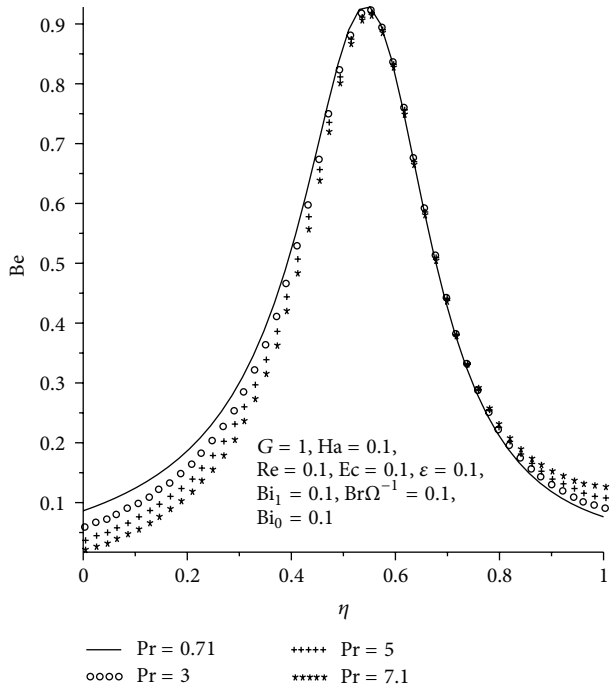

Figure 30: Bejan number with increasing Pr.

conditions enhance the dominant effects of heat transfer irreversibility on the flow system. An increase in the pressure gradient parameter causes a decrease in the Bejan number within the channel leading to an increase in the irreversibility due to fluid friction as shown in Figure 29. Figure 30 shows that the Bejan number slightly decreases at the lower plate and slightly increases at the upper plate with increasing Prandtl number Pr.

5. Conclusion

In this paper, the effects of magnetic field on variable viscosity channel flow with suction/injection together with convective heating/cooling at the walls have been investigated. The nonlinear model problem is tackled numerically using shooting quadrature and fourth-order Runge-Kutta iteration scheme. Based on the results presented above, the following conclusions are deduced.

(i) An increase in ε, Ec, G, Pr, and Bi_0 increases the velocity profiles, while an increase in Ha and Bi_1 decreases the velocity profile along channel centerline region.

(ii) An increase in ε, Ec, G, Pr, Re, and Bi_0 increases the temperature profiles, while an increase in Ha and Bi_1 decreases the temperature profile.

(iii) An increase in ε, Bi_0, Bi_1, G, and $\mathrm{Br}\Omega^{-1}$ increases the entropy generation rate. An increase in Re decreases Ns at injection wall, while at suction wall Ns increases. An increase in Ha increases Ns at both walls but decreases Ns at centre of the channel.

(iv) An increase in ε, G, $\mathrm{Br}\Omega^{-1}$, and Ha decreases the Be with increasing fluid friction and magnetic field irreversibility. An increase in Pr decreases Be at injection wall but increases Be at suction wall. Meanwhile increase in Bi_0, Bi_1 increases the Be with increasing effect of heat transfer irreversibility.

Nomenclature

C_p: Specific heat at a constant pressure
u: Fluid velocity
V: Uniform suction/injection velocity
T: Fluid temperature
Be: Bejan number
T_f: Hot fluid temperature
h: Channel width
Re: Reynolds number
Br: Brinkmann number
(x, y): Cartesian coordinates
X: Dimensionless axial coordinate
Bi_0: Lower plate Biot number
m: Variable viscosity parameter
k: Thermal conductivity
P: Fluid pressure
E_G: Volumetric rate of entropy
Ha: Square of Hartmann number
T_∞: Ambient temperature
G: Pressure gradient
Pr: Prandtl number
Ec: Eckert number
w: Dimensionless velocity
B_0: Magnetic field strength
Bi_1: Upper plate Biot number.

Greek Symbols

α: Thermal diffusivity
θ: Dimensionless temperature
Ω: Temperature difference parameter
η: Dimensionless transverse coordinate
$\overline{\mu}(T)$: Temperature dependent viscosity
μ_0: Fluid viscosity at ambient temperature
μ: Fluid viscosity
ϕ: Irreversibility ratio
ρ: Fluid density
σ: Electrical conductivity
γ_0: Lower plate heat transfer coefficient
γ_1: Upper plate heat transfer coefficient.

References

[1] R. Moreau, *Magnetohydrodynamics*, Kluwer Academic Publishers, Dordrecht, The Netherlands, 1990.

[2] J. Hartmann and F. Lazarus, "Kongelige danske videnskabernes selskab," *Matematisk-Fysiske Meddelelser*, vol. 15, pp. 6–7, 1937.

[3] G. W. Sutton and A. Sherman, *Engineering Magnetohydrodynamics*, McGraw Hill, 1965.

[4] Y. Liu, L. Zheng, and X. Zhang, "Unsteady MHD Couette flow of a generalized Oldroyd-B fluid with fractional derivative," *Computers and Mathematics with Applications*, vol. 61, no. 2, pp. 443–450, 2011.

[5] B. Lehnert, "On the behaviour of an electrically conductive liquid in a magnetic field," *Arkiv för Fysik*, vol. 5, no. 5, pp. 69–90, 1952.

[6] O. D. Makinde and P. Y. Mhone, "Heat transfer to MHD oscillatory flow in a channel filled with porous medium," *Romanian Journal of Physics*, vol. 50, no. 9-10, pp. 931–938, 2005.

[7] G. S. Seth, M. S. Ansari, and R. Nandkeolyar, "Unsteady hydromagnetic couette flow within a porous channel," *Tamkang Journal of Science and Engineering*, vol. 14, no. 1, pp. 7–14, 2011.

[8] J. P. Agarwal, "On generalized incompressible couette flow in hydromagnetics," *Applied Scientific Research B*, vol. 9, no. 4-5, pp. 255–266, 1962.

[9] O. D. Makinde and O. O. Onyejekwe, "A numerical study of MHD generalized Couette flow and heat transfer with variable viscosity and electrical conductivity," *Journal of Magnetism and Magnetic Materials*, vol. 323, no. 22, pp. 2757–2763, 2011.

[10] A. Bejan, "Second-law analysis in heat transfer and thermal design," *Advances in Heat Transfer*, vol. 15, pp. 1–58, 1982.

[11] L. C. Wood, *Thermodynamics of Fluid Systems*, Oxford University Press, Oxford, UK, 1975.

[12] G. Ibanez, S. Cuevas, and M. Lopez de Haro, "Minimization of entropy generation by asymmetric convective cooling," *International Journal of Heat and Mass Transfer*, vol. 46, pp. 1321–1328, 2003.

[13] S. Mahmud and R. A. Fraser, "Flow, thermal, and entropy generation characteristics inside a porous channel with viscous dissipation," *International Journal of Thermal Sciences*, vol. 44, no. 1, pp. 21–32, 2005.

[14] A. Z. Sahin and R. Ben-Mansour, "Entropy generation in laminar fluid flow through a circular pipe," *Entropy*, vol. 5, no. 5, pp. 404–416, 2003.

[15] K. Hooman, "Entropy generation for microscale forced convection: effects of different thermal boundary conditions, velocity slip, temperature jump, viscous dissipation, and duct geometry," *International Communications in Heat and Mass Transfer*, vol. 34, no. 8, pp. 945–957, 2007.

[16] A. S. Eegunjobi and O. D. Makinde, "Effects of Navier slip on entropy generation in a porous channel with suction/injection," *Journal of Thermal Science and Technology*, vol. 7, no. 4, pp. 522–535, 2012.

[17] O. D. Makinde and A. S. Eegunjobi, "Effects of convective heating on entropy generation rate in a channel with permeable Walls," *Entropy*, vol. 15, pp. 220–233, 2013.

[18] M. Turkyilmazoglu, "Heat and mass transfer of MHD second order slip flow," *Computers & Fluids*, vol. 71, pp. 426–434, 2013.

[19] T. Y. Na, *Computational Methods in Engineering Boundary Value Problems*, Academic Press, New York, NY, USA, 1979.